Advances in Nano Research, *Vol. 2, No. 3 (2014) 157-172*
DOI: http://dx.doi.org/10.12989/anr.2014.2.3.157

Atomistic simulation of surface passivated wurtzite nanowires: electronic bandstructure and optical emission

Vinay U. Chimalgi, Md Rezaul Karim Nishat, Krishna K. Yalavarthi and Shaikh S. Ahmed*

Department of Electrical and Computer Engineering, Southern Illinois University at Carbondale, 1230 Lincoln Drive, Carbondale, IL 62901, USA

(Received July 31, 2014, Revised December 22, 2014, Accepted December 24, 2014)

Abstract. The three-dimensional Nano-Electronic Modeling toolkit (NEMO 3-D) is an *open source* software package that allows the *atomistic* calculation of single-particle electronic states and optical response of various semiconductor structures including bulk materials, quantum dots, impurities, quantum wires, quantum wells and nanocrystals containing *millions of atoms*. This paper, first, describes a software module introduced in the NEMO 3-D toolkit for the calculation of electronic bandstructure and interband optical transitions in nanowires having *wurtzite* crystal symmetry. The energetics (Hamiltonian) of the quantum system under study is described via the tight-binding (TB) formalism (including sp^3, sp^3s^* and $sp^3d^5s^*$ models as appropriate). Emphasis has been given in the treatment of surface atoms that, if left unpassivated, can lead to the creation of energy states within the bandgap of the sample. Furthermore, the developed software has been validated via the calculation of: a) modulation of the energy bandgap and the effective masses in [0001] oriented wurtzite nanowires as compared to the experimentally reported values in bulk structures, and b) the localization of wavefunctions and the optical anisotropy in GaN/AlN disk-in-wire nanowires.

Keywords: NEMO 3-D; atomistic simulation; tight-binding; Wurtzite nanowire; optical anisotropy; internal fields; electronic structure

1. Introduction

In the last decade, nanowires (NWs) made from a wide variety of materials have drawn considerable interest. Especially, the group-III nitride material system has been the subject of intense experimental and theoretical research mainly due to their wide range of emission frequencies, high stability against defects, high temperature and potential for applications in various optoelectronic, solid-state lighting, and high-mobility electronic devices (Ponce and Bour 1997). With the use of nanowires in these devices, the performance is enhanced due to increased charge localization and reduction in the defect density (Merill et al. 2012). For example, recently, much progress has been made in developing piezoelectric nano-generators using wurtzite InN (Huang et al. 2010), CdS (Lin et al. 2008), ZnS (Lu et al. 2009) nanowires. High performance

*Corresponding author, Professor, E-mail: ahmed@siu.edu

Copyright © 2014 Techno-Press, Ltd.
http://www.techno-press.com/?journal=anr&subpage=7 ISSN: 2287-237X (Print), 2287-2388 (Online)

logic circuits using CdS NWS (Ma *et al.* 2007) have been proposed. Also, because of their excellent mechanical properties, high chemical resistivity, and wide bandgap, GaN and SiC NWs are attractive candidates for applications in high power, high frequency, high temperature and harsh environments.

Knowledge of *electronic bandstructure* of nanostructures is an essential step towards the understanding of device performance and reliable device design. For example, the *energy bandgaps* and the *effective masses* are important physical parameters that determine the transport properties of charge carries in low dimensionality structures. Due to strong quantum confinement effects in extremely thin 1-D NWs, the electronic and optical properties exhibit certain unconventional features as compared to bulk (3-D) and thin-film (2-D) counterparts, which consequently affect the device characteristics.

This paper, first, describes a software module introduced in the NEMO 3-D toolkit for the calculation of electronic bandstructure and interband optical transitions in *surface passivated* [0001] oriented nanowires having *wurtzite* crystal symmetry. The energetics (Hamiltonian) of the quantum system is described via the tight-binding (TB) formalism (including sp^3, sp^3s^* and $sp^3d^5s^*$ models as appropriate). The physical structure of the nanowire is constructed by repeating the *supercell* along the growth direction. The corresponding Hamiltonian is constructed from the atomistic structural representation. Finally, the electronic dispersion (bandstructure) is obtained by solving the eigenvalue problem (that is, diagonalization of the Hamiltonian). Next, the developed software has been validated via the calculation of: a) modulation of the energy bandgap and the effective masses in [0001] oriented wurtzite nanowires as compared to the experimentally reported values in bulk structures, and b) the localization of wavefunctions and the optical anisotropy in GaN/AlN disk-in-wire nanowires.

2. NEMO 3-D in a nutshell

The three-dimensional Nano-Electronic Modeling toolkit (NEMO 3-D) is an *open source* software package that allows the calculation of single-particle electronic states and optical response of various semiconductor structures including bulk materials, quantum dots, impurities, quantum wires, quantum wells and nanocrystals. Detail description of this package can be found in Klimeck *et al.* (2002), Ahmed *et al.* (2009), Klimeck *et al.* (2007), Ahmed *et al.* (2007), Ahmed *et al.* (2010), Ahmed *et al.* (2011) and Usman *et al.* (2011). NEMO 3-D bridges the gap between the *large* size (millions of atom) classical semiconductor device models and the *molecular* level (few atoms) modeling. NEMO 3-D currently enables the computation of electronic structure using a variety of tight-binding models (s, sp^3s^*, $sp^3d^5s^*$) that are optimized with a genetic algorithm tool. Whereas, for the calculation of *atomistic* (non-linear) strain relaxation, NEMO 3-D currently employs the atomistic valence-force field (VFF) with strain-dependent Keating potentials (Keating 1966). From the single-particle eigenstates various physical properties can be calculated in NEMO 3-D such as optical matrix elements, Coulomb and exchange matrix elements, approximate single cell bandstructures from supercell bandstructure. Effects of interaction with external electromagnetic fields are also included. NEMO 3-D includes spin in its fundamental atomistic tight binding representation. The complexity and generality of physical models in NEMO 3-D can place high demands on computational resources. For example, in the 20-band electronic calculation the discrete Hamiltonian matrix is of order 20 times the number of atoms. Thus, in a computation with 20 million atoms, the matrix is of order 400 million. Computations of that size

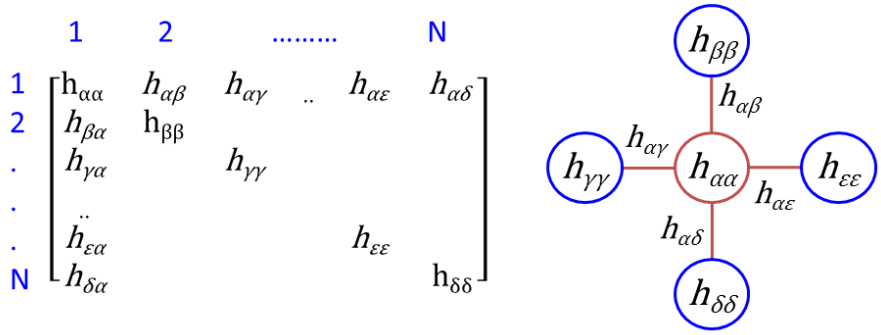

(a) (b)

Fig. 1 (a) Hamiltonian matrix representation for *N* number of atoms. (b) Connectivity of a single atom with 4 (four) bonds.

can be handled because of the parallelized design of the package. NEMO 3-D is implemented in ANSI C, C++ with MPI used for message-passing, which ensures its portability to all major high-performance computing platforms, and allows for an efficient use of distributed memory and parallel execution mechanisms. New features of NEMO 3-D include 3-D domain decomposition parallelism. The algorithms/solvers available in NEMO 3-D include the PARPACK library, a custom implementation of the Lanczos method, Block Lanczos method, the spectrum folding method and the Tracemin method. Recent benchmarks show (Haley *et al.* 2009) that 3-D domain decomposition scheme can be utilized exceeding 32,000 cores on realistic electronic structures comprised of one billion atoms. We are not aware of any other semiconductor device simulation code that can simulate such large number of atoms!

3. Software development in NEMO 3-D for wurtzite symmetry

3.1 Atomistic representation of the physical structure

The supercell of a nanowire is constructed by repeating the unit cell until the specified size (area) is obtained (for example) in *x* and *y* directions and with periodicity in *z*-direction. Once the supercell is constructed, the location of the atoms and the direction of the bonds are extracted and are stored in a *connectivity matrix*. For every atom, the direction and length of each bond is identified with the help of this matrix. In order to calculate the bandstructure, the atoms with open bonds in *z*-direction are subjected to periodic boundary conditions. Even after applying periodic boundary conditions, there still exists a condition where any of the 4 (four) bonds of an atom is not connected to its neighbor (generally reaching outside its surface area). Such an atom is referred to as *surface atom*. These unconnected (dangling) bonds have to be passivated so that they do not participate in bandstructure calculation.

3.2 Construction of Hamiltonian matrix

The Hamiltonian is constructed atom-by-atom as they appear in the nanowire by sweeping the rows (*x*-direction) and columns (*y*-direction) over the entire cross section. The approach is similar

Table 1 Basis information for various band models

Band Model	Basis, n_b	
	W/out spin	With spin
sp^3	4	8
sp^3s^*	10	20
$sp^3d^5s^*$	20	40

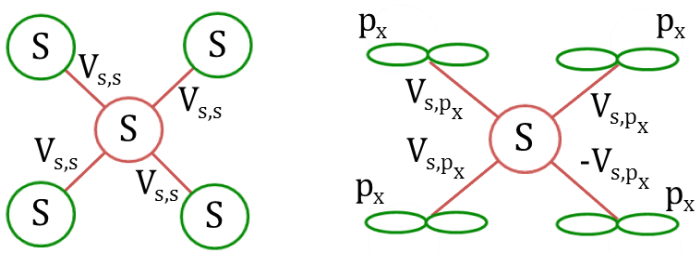

Fig. 2 Example of sign/parity coupling between *s*-*s* and *s*-p_x orbitals for all four bonds.

to that employed in a zincblende lattice as has been described in details in Neophytou (2008). Based on the two-center approximation, each atom in the Hamiltonian matrix is modeled by a diagonal (on-site) term ($h_{\alpha\alpha}$) and four off-diagonal (connectivity or interaction) terms ($h_{\alpha\beta}$, $h_{\alpha\gamma}$, $h_{\alpha\delta}$, $h_{\alpha z}$), as shown in Fig. 1. Note that the diagonal and the off-diagonal terms are further represented by matrices of size $n_b \times n_b$, where n_b is the dimension of the tight-binding basis set. Therefore, the size of the Hamiltonian matrix depends on both the number of atoms, N, in the nanowire and the corresponding basis sets, n_b, used and is given by ([N*n_b]×[N*n_b]). The dimension of the basis set depends on the selected band model which is listed in Table 1. In case of a *surface atom*, the diagonal element of an atom associated with the dangling bond should be *passivated*.

As an example, a two-atom (*anion* and *cation*) Hamiltonian construction is described via the following matrix

$$H = \begin{bmatrix} H_{aa} & H_{ac} \\ H_{ca} & H_{cc} \end{bmatrix} \tag{1}$$

where, H_{aa} and H_{cc} are the on-site elements for *anion* and *cation* orbitals, respectively, and the coupling between the two atoms is represented by the off-diagonal elements (H_{ac} and H_{ca}). Here, $H_{aa}=[E_{i,j}]\delta_{i,j}$ and $H_{ac} = \left[G_{i,j}V_{i,j}^{ac}\right]$, with i, j running through the orbital indexes for the 10-band model (s, p_x, p_y, p_z, s^*). In the above equation, the cation-to-anion coupling matrix, H_{ca}, has an order of [n_b*n_b]). The total Hamiltonian matrix H is hermitian, since H_{ac} is defined as $H_{ac} = H_{ac}^T$. Also, V_{ij} is given by (Neophytou 2008)

$$V_{i,j}^{a,c} = f_{i,j}(l,m,n)V_{u,v} \tag{2}$$

where, $f_{i,j}(l,m,n)$ are the two center Slater-Koster integrals (Slater and Koster 1954) that transforms the orthogonal Lowdin (1950) based described orbitals into the σ, π and δ bonding, (l,m,n) are the directional cosines of the lattice, and $V_{u,v}$ are the tight binding fitting parameters. The element $G_{i,j}$ represents the sign matrix of size [n_b*n_b], and is unique for each bond. This matrix

consists of coupling of $V_{s,s}$, V_{s,p_x} , V_{s,p_y} , and V_{s,p_z} orbitals that are different for each bond, which is illustrated in Fig. 2. For all the bonds between the anion and cations, although the *magnitude* of the matrix is same, the *sign* of the individual element in the matrix changes according to the bond considered.

3.3 Surface passivation

The dangling bonds are passivated using the sp^3 hybridization technique. The onsite elements in the Hamiltonian have contributions from all four bonds that assume the individual orbitals as the basis set. A *transformation* from the orbital space to the hybridized space is then performed to passivate a particular dangling bond. The entries (bases) in the transformed matrix represent the bonds, which captures the contribution from all relevant orbitals. The open bonds that are to be passivated are assigned high energy values (such as 30 eV) so that they do not participate in the bandstructure calculation. In general, the algebraic expression for sp^3-hybridized atomic orbitals (Hosoya *et al.* 1998) is a *linear combination* of *s* and *p* orbitals and is given as

$$\begin{aligned}
\chi_{3,1} &= \frac{1}{2}s + \frac{\sqrt{3}}{2}p_x \\
\chi_{3,2} &= \frac{1}{2}s - \frac{1}{\sqrt{12}}p_x + \frac{\sqrt{2}}{3}p_y \\
\chi_{3,3} &= \frac{1}{2}s - \frac{1}{\sqrt{12}}p_x - \frac{1}{\sqrt{6}}p_y + \frac{1}{\sqrt{2}}p_z \\
\chi_{3,3} &= \frac{1}{2}s - \frac{1}{\sqrt{12}}p_x - \frac{1}{\sqrt{6}}p_y - \frac{1}{\sqrt{2}}p_z
\end{aligned} \tag{3}$$

Wurtzite crystals consist of 4 atoms in a unit cell (i.e., 2 cations and 2 anions). Using the sp^3 hybridization scheme, the bonds corresponding to each atom is represented as follows:

Cation I

$$\begin{aligned}
\left|sp^3\right\rangle_{[001]} &= \left|s\right\rangle + \left|p_x\right\rangle + \left|p_y\right\rangle + \left|p_z\right\rangle \\
\left|sp^3\right\rangle_{[0\bar{1}\bar{1}]} &= \left|s\right\rangle + \left|p_x\right\rangle - \left|p_y\right\rangle - \left|p_z\right\rangle \\
\left|sp^3\right\rangle_{[\bar{1}1\bar{1}]} &= \left|s\right\rangle - \left|p_x\right\rangle + \left|p_y\right\rangle - \left|p_z\right\rangle \\
\left|sp^3\right\rangle_{[1\bar{1}\bar{1}]} &= \left|s\right\rangle + \left|p_x\right\rangle + \left|p_y\right\rangle - \left|p_z\right\rangle
\end{aligned} \tag{4}$$

$$\begin{bmatrix} \left|sp^3\right\rangle_{[001]} \\ \left|sp^3\right\rangle_{[0\bar{1}\bar{1}]} \\ \left|sp^3\right\rangle_{[\bar{1}1\bar{1}]} \\ \left|sp^3\right\rangle_{[1\bar{1}\bar{1}]} \end{bmatrix} = \begin{bmatrix} 0.5 & 0 & 0 & \sqrt{3}/2 \\ 0.5 & 0 & -\sqrt{6}/3 & -\sqrt{3}/6 \\ 0.5 & -1/\sqrt{2} & 1/\sqrt{6} & -\sqrt{3}/6 \\ 0.5 & 1/\sqrt{2} & 1/\sqrt{6} & -\sqrt{3}/6 \end{bmatrix} \begin{bmatrix} \left|s\right\rangle \\ \left|p_x\right\rangle \\ \left|p_y\right\rangle \\ \left|p_z\right\rangle \end{bmatrix} = U_{sp^3} \tag{5}$$

Similarly for Cation II

$$\begin{aligned}
\left|sp^3\right\rangle_{[001]} &= |s\rangle + |p_x\rangle + |p_y\rangle + |p_z\rangle \\
\left|sp^3\right\rangle_{[01\bar{1}]} &= |s\rangle + |p_x\rangle + |p_y\rangle - |p_z\rangle \\
\left|sp^3\right\rangle_{[\bar{1}\bar{1}1]} &= |s\rangle - |p_x\rangle - |p_y\rangle - |p_z\rangle \\
\left|sp^3\right\rangle_{[\bar{1}1\bar{1}]} &= |s\rangle + |p_x\rangle - |p_y\rangle - |p_z\rangle
\end{aligned} \tag{6}$$

$$\begin{bmatrix} \left|sp^3\right\rangle_{[001]} \\ \left|sp^3\right\rangle_{[01\bar{1}]} \\ \left|sp^3\right\rangle_{[\bar{1}\bar{1}1]} \\ \left|sp^3\right\rangle_{[\bar{1}1\bar{1}]} \end{bmatrix} = \begin{bmatrix} 0.5 & 0 & 0 & \sqrt{3}/2 \\ 0.5 & 0 & \sqrt{6}/3 & -\sqrt{3}/6 \\ 0.5 & 1/\sqrt{2} & -1/\sqrt{6} & -\sqrt{3}/6 \\ 0.5 & -1/\sqrt{2} & -1/\sqrt{6} & -\sqrt{3}/6 \end{bmatrix} \begin{bmatrix} |s\rangle \\ |p_x\rangle \\ |p_y\rangle \\ |p_z\rangle \end{bmatrix} = U_{sp^3} \tag{7}$$

Anion I

$$\begin{aligned}
\left|sp^3\right\rangle_{[00\bar{1}]} &= |s\rangle + |p_x\rangle + |p_y\rangle - |p_z\rangle \\
\left|sp^3\right\rangle_{[0\bar{1}1]} &= |s\rangle + |p_x\rangle - |p_y\rangle + |p_z\rangle \\
\left|sp^3\right\rangle_{[\bar{1}11]} &= |s\rangle - |p_x\rangle + |p_y\rangle + |p_z\rangle \\
\left|sp^3\right\rangle_{[111]} &= |s\rangle + |p_x\rangle + |p_y\rangle + |p_z\rangle
\end{aligned} \tag{8}$$

$$\begin{bmatrix} \left|sp^3\right\rangle_{[00\bar{1}]} \\ \left|sp^3\right\rangle_{[0\bar{1}1]} \\ \left|sp^3\right\rangle_{[\bar{1}11]} \\ \left|sp^3\right\rangle_{[111]} \end{bmatrix} = \begin{bmatrix} 0.5 & 0 & 0 & -\sqrt{3}/2 \\ 0.5 & 0 & -\sqrt{6}/3 & \sqrt{3}/6 \\ 0.5 & -1/\sqrt{2} & 1/\sqrt{6} & \sqrt{3}/6 \\ 0.5 & 1/\sqrt{2} & 1/\sqrt{6} & \sqrt{3}/6 \end{bmatrix} \begin{bmatrix} |s\rangle \\ |p_x\rangle \\ |p_y\rangle \\ |p_z\rangle \end{bmatrix} = U_{sp^3} \tag{9}$$

Anion II

$$\begin{aligned}
\left|sp^3\right\rangle_{[00\bar{1}]} &= |s\rangle + |p_x\rangle + |p_y\rangle - |p_z\rangle \\
\left|sp^3\right\rangle_{[011]} &= |s\rangle + |p_x\rangle + |p_y\rangle + |p_z\rangle \\
\left|sp^3\right\rangle_{[1\bar{1}1]} &= |s\rangle + |p_x\rangle - |p_y\rangle + |p_z\rangle \\
\left|sp^3\right\rangle_{[\bar{1}\bar{1}1]} &= |s\rangle - |p_x\rangle - |p_y\rangle + |p_z\rangle
\end{aligned} \tag{10}$$

$$\begin{bmatrix} \left|sp^3\right\rangle_{[00\bar{1}]} \\ \left|sp^3\right\rangle_{[011]} \\ \left|sp^3\right\rangle_{[1\bar{1}1]} \\ \left|sp^3\right\rangle_{[\bar{1}\bar{1}1]} \end{bmatrix} = \begin{bmatrix} 0.5 & 0 & 0 & -\sqrt{3}/2 \\ 0.5 & 0 & \sqrt{6}/3 & \sqrt{3}/6 \\ 0.5 & 1/\sqrt{2} & -1/\sqrt{6} & \sqrt{3}/6 \\ 0.5 & -1/\sqrt{2} & -1/\sqrt{6} & \sqrt{3}/6 \end{bmatrix} \begin{bmatrix} \left|s\right\rangle \\ \left|p_x\right\rangle \\ \left|p_y\right\rangle \\ \left|p_z\right\rangle \end{bmatrix} = U_{sp^3} \tag{11}$$

Analytical procedure for surface passivation (Neophytou 2008) is described in the following:

(1) The transformation from orbital to hybridized space is carried out by employing the following transformation equation

$$\left[H\right]_{hybrid} = U_{sp^3}\left[H\right]_{orbital} U_{sp^3}^T \tag{12}$$

where, U_{sp^3} is transformation matrix and defined in above equations. The $[H]_{orbital}$ matrix consists of onsite elements which is given by

$$H_{orbital} = \begin{bmatrix} E_s & & & \\ & E_{p_x} & & \\ & & E_{p_y} & \\ & & & E_{pz} \end{bmatrix} \tag{13}$$

where, E_s, E_{p_x}, E_{p_y}, E_{p_z} are the onsite orbital energies.

(2) A high energy of ~30 eV is applied to the dangling bonds that are to be passivated and is added to the hybridized matrix ($[H]_{orbital}$) as follows

$$\left[H\right]_{hybrid} = \left[H\right]_{hybrid} + \left[H\right]_{sp3} \tag{14}$$

$$H_{sp^3} = \begin{bmatrix} b_1 & & & \\ & b_2 & & \\ & & b_3 & \\ & & & b_4 \end{bmatrix} \tag{15}$$

where, b_1 to b_4 represent the atomic bonds with 'b_i' being 0 eV for connected bonds and 30 eV for dangling bonds.

(3) Finally, a back transformation is performed from the hybridized space to orbital space, and the corresponding correction matrix ($[H_E]_{correction}$) is given by

$$\left[H_E\right]_{correction} = U_{sp^3}^T\left[H_{hybrid}\right]U_{sp^3} \tag{16}$$

4. Calculation of electronic bandstructure

We considered Wurtzite nanowires that are confined in the x and y directions and periodic

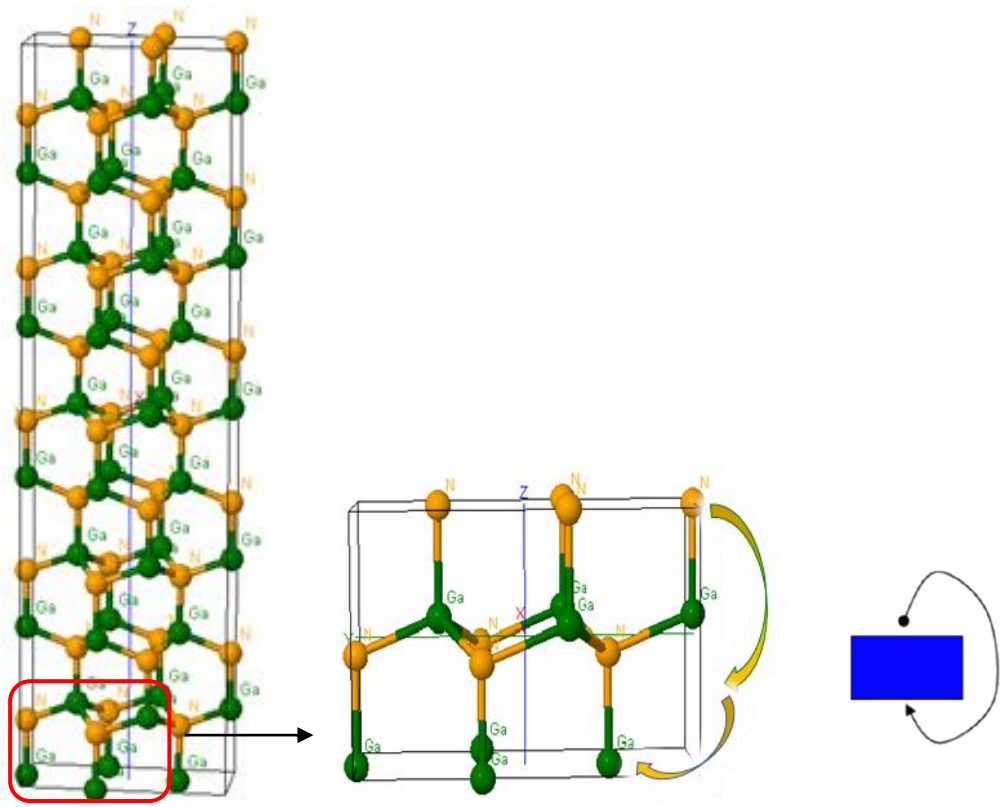

Fig. 3 (left) GaN nanowire with a cross-section of 0.7 nm×0.7 nm and periodicity in the *z*-direction that is along [0001]. (middle) Supercell representation. (right) Block representation of the supercell with periodic boundary condition

along the *z*-direction. Fig. 3 shows a GaN nanowire having thickness 0.7 nm and periodicity in the *z*-direction [0001]. To treat/model the periodicity, atoms in the top *z*-plane of the surface are considered to have its bonds connected to the atoms in the bottom *z* plane, such that the structure repeats itself along the *z*-direction [0001]. In this case, the nitrogen atom, *N* on the top has bond connecting to a gallium atom on the bottom as shown in Fig. 3.

The importance of passivation of dangling bonds is delineated in the following for a GaN nanowire having a cross section of 2 nm × 2 nm and periodicity along the [0001] direction. Fig. 4 shows the calculated energy bandstructure for the nanowire with *unpassivated* surface atoms using the sp^3s^* tight-binding model. Here the energy state formed at around 1.35 eV clearly emanates from the unpassivated characteristic of the dangling bonds at the surface. With appropriate bond passivation energy (for example, ~30 eV in this case), as shown in Fig. 5, this surface state is completely eliminated.

Fig. 6 shows the variation of the *direct* energy bandgap and the Gamma-valley effective masses calculated for [0001] oriented GaN, InN, AlN, 2H-SiC, ZnSe and CdSe nanowires all having a wurtzite crystal symmetry. The bandgap and the effective masses in nanowires are found to be deviating from those of bulk counterparts, and are a strong function of nanowire dimension (diameter/base side). The increase in the energy bandgap and the Gamma valley effective mass

with the reduction of nanowire dimension is due to the quantum-mechanical size-quantization effect and non-parabolicity presence in the electronic dispersion, respectively. Also, the quantum confinement effect is found to be significantly strong for nanowires having a diameter/base side of less than 3 nm.

5. Optical emission in GaN/AlN disk-in-wire structure

A GaN disk when sandwiched between nanostructured (nanowire) AlN substrate and cap layers forms a so called disk-in-wire structure. The use of nanowires as the active region in a light emitter

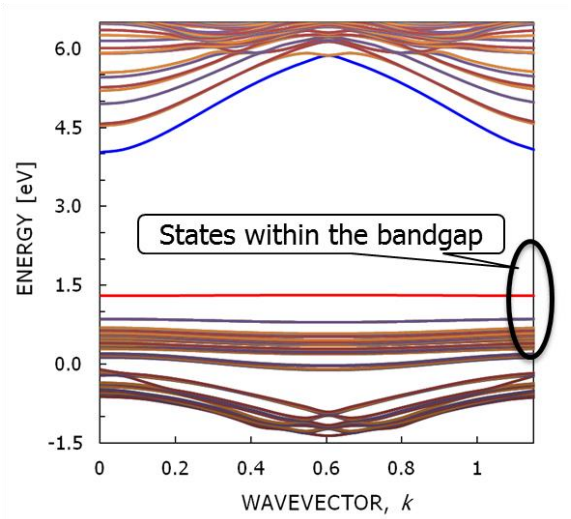

Fig. 4 Bandstructure of *unpassivated* [0001] oriented GaN nanowire (thickness ~2 nm)

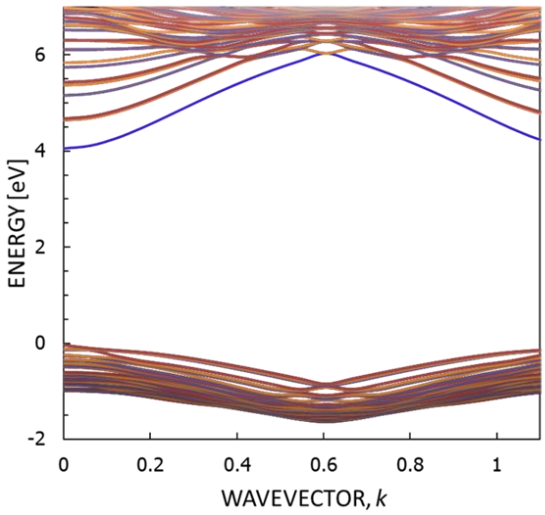

Fig. 5 Bandstructure of *passivated* [0001] oriented GaN nanowire (thickness ~2 nm)

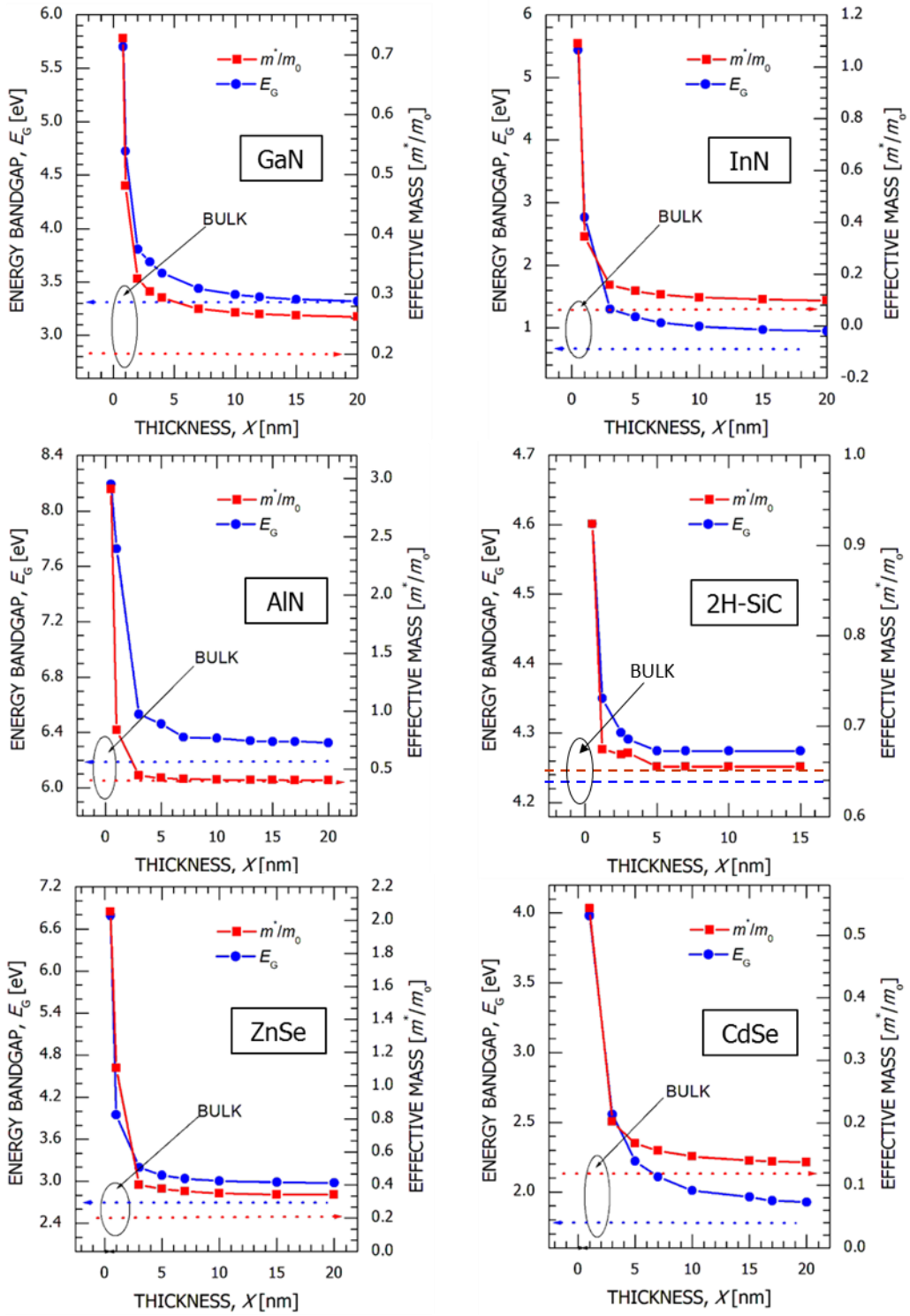

Fig. 6 Electronic bandstructure of [0001]-oriented GaN, InN, AlN, 2H-SiC, ZnSe and CdSe wires

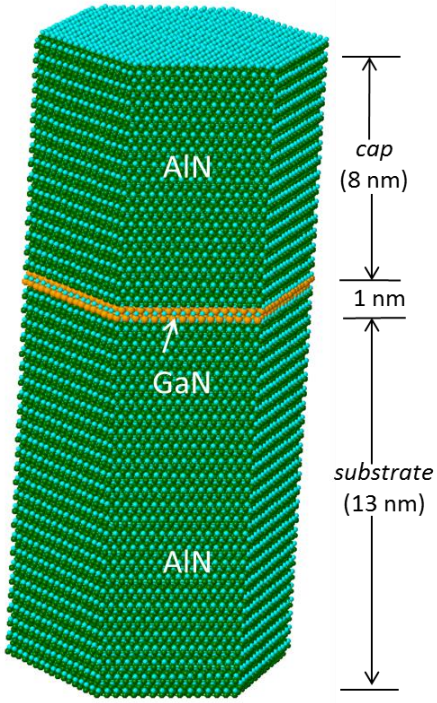

Fig. 7 Atomistic representation of the AlN/GaN/AlN quantum disk-in-a-wire structure

leads to lower concentration of defects, allowing for higher levels of lattice mismatch and more design freedom in bandgap engineering than possible in conventional bulk and thin-film QW heterostructures. These nanostructures, therefore, are strong candidates for UV and near-IR applications (Prodhomme *et al.* 2013). However, the wurtzite crystal symmetry in these dots induces internal fields arising from (Bardoux *et al.* 2008): a) crystal atomicity, b) strained inner region, c) piezoelectricity, and d) spontaneous polarization (pyroelectricity). In this Section, using the modified NEMO 3-D simulator and appropriate post-processing tools, we study the anisotropic characteristic of interband optical emissions in a wurtzite AlN/GaN/AlN disk-in-wire structure.

Fig. 7 shows the simulated wurtzite AlN/GaN/AlN disk-in-a-wire structure. The supporting AlN nanowire is grown in the [0001] direction (*c*-axis) with base length, *d*~10 nm and height, *h*~22 nm. The GaN quantum disk is positioned on the AlN substrate and has a height of *h*~1 nm. In the strain calculation, the equilibrium atomic positions are determined by minimizing the total elastic energy of the system employing an atomistic valence force-field (VFF) method. From our calculations, as shown in the 1-D strain profiles in Fig. 8(a), the hydrostatic strain ($\varepsilon_{xx}+\varepsilon_{yy}+\varepsilon_{zz}$) is found to be compressive within the disk and tensile in the substrate and cap layers. The biaxial strain is found to be tensile at the middle of the disk. Fig. 8(b) shows the 1-D off-diagonal strain profile along the center of the structure. Here, ε_{xz} and ε_{yz} were found to be large having maxima at the AlN/GaN interfaces, whereas ε_{xy} is comparatively small in the disk region. Overall, atomistic strain was found to be long-ranged stressing the need for using realistically-extended structures in modeling these devices.

Next, the calculation of the internal electrostatic fields is carried out using an approach

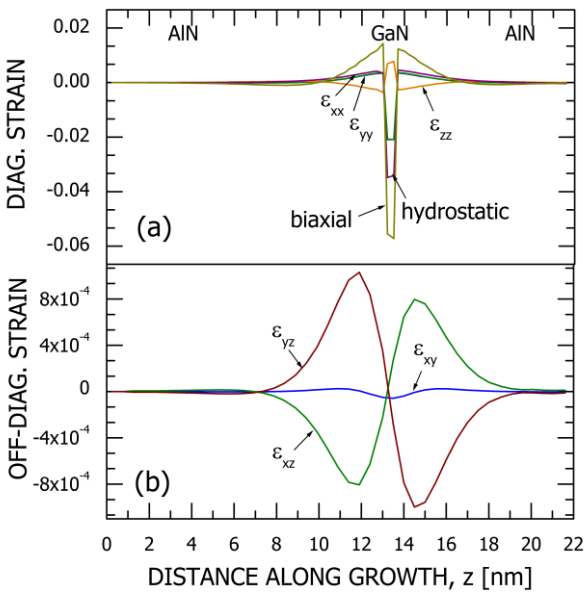

Fig. 8 Atomistic (a) diagonal and (b) off-diagonal strain distributions along the growth ([0001]) direction through the center of the disk. Strain is found to penetrate deep into the substrate and the cap layers

described in Sundaresan *et al.* (2014), Yalavarthi *et al.* (2014), Merrill *et al.* (2012). The overall polarization **P** in a typical wurtzite semiconductor is given by $\mathbf{P}=\mathbf{P}_{PZ}+\mathbf{P}_{SP}$, where $\mathbf{P}_{PZ}$ is the strain-induced piezoelectric polarization and $\mathbf{P}_{SP}$ is the spontaneous polarization (pyroelectricity). The piezoelectric polarization $\mathbf{P}_{PZ}$ is obtained from the diagonal and shear components of the anisotropic *atomistic* strain fields. In contrast, the spontaneous polarization is strain-independent and arises from fundamental asymmetry of the crystal structure. However, it is well known that the piezoelectric polarization is generally a *non-linear* function of strain, the non-linearity becoming important for large epitaxial strains. Following a very recent work of Prodhomme *et al*. (2013), recently a model for the second-order polarization effects in wurtzite material systems has been implemented in this work. In Prodhomme *et al*. (2013), to calculate the second-order piezoelectric coefficients, the authors have used a finite difference technique in conjunction with density functional perturbation theory (DFPT) within the local density approximation (LDA). It was found that the second-order piezoelectric effects in crystals with wurtzite symmetry can lead to corrections of the order of 15% in quantum wells and up to 40% for epitaxial quantum dots. The net piezoelectric polarization (including the first-order and the second-order contributions) along the [0001] direction in a wurtzite crystal is given by

$$P_z^{net} = e_{31}\left(\varepsilon_{xx}+\varepsilon_{yy}\right)+e_{33}\varepsilon_{zz}+\frac{1}{4}\left(e_{311}+e_{312}\right)\left(\varepsilon_{xx}+\varepsilon_{yy}\right)^2+\frac{1}{2}e_{333}\varepsilon_{zz}^2+2e_{313}\varepsilon_{xx}\varepsilon_{zz} \tag{17}$$

The polarization constants (in C/m^2) used in this study are obtained from Prodhomme *et al*. (2013) and given in Table 2. It was found that the second-order polarization coefficients are almost an order of magnitude larger than the linear counterparts. Also, of all the coefficients, e_{333} has the largest magnitude and can induce significant second-order effects especially in materials with a

Table 2 Polarization Constants (in C/m^2) for AlN and GaN (Prodhomme *et al.* 2013)

	1st-order			2nd-order				P_{SP} (C/m^2)
	e_{15}	e_{31}	e_{33}	e_{311}	e_{312}	e_{313}	e_{333}	
GaN	-0.31	-0.44	0.75	6.2	3.3	0.4	-21.4	-0.027
AlN	-0.35	-0.67	1.67	3.0	3.0	3.8	-26.0	-0.095

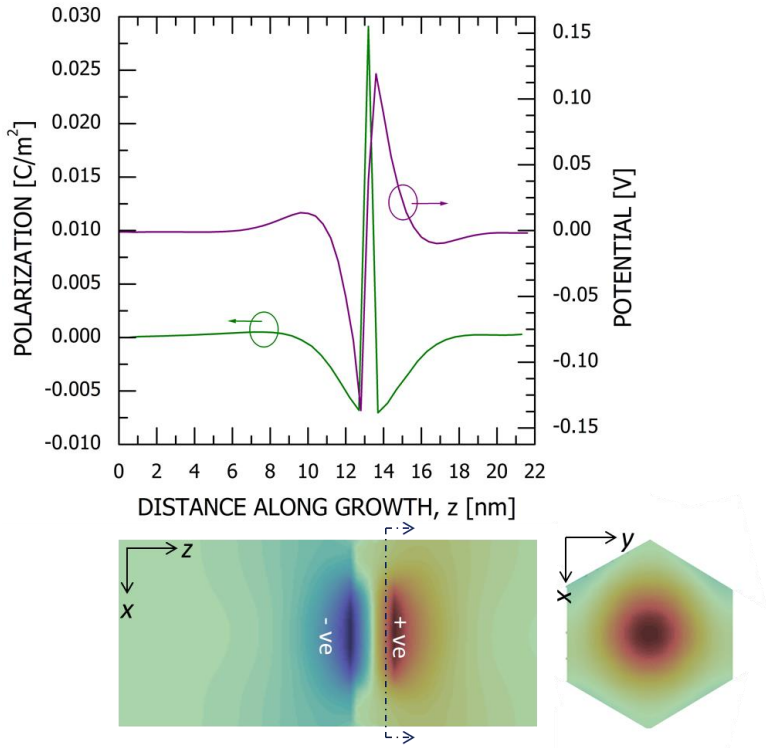

Fig. 9 (top) Net (including both piezoelectric and pyroelectric contributions) polarization and the induced potential distributions along the [0001] direction. Note the large spread of the potential in the substrate and the cap layers. (bottom) Potential distribution in the *x-y* and *x-z* planes halfway through the disk

rather small linear coefficient e_{33}. The net polarization and the induced potential distributions in the [0001] direction are shown in Fig. 9. Lower panels of this figure shows the 2-D potential distributions projected in the XY and XZ planes, revealing pronounced anisotropy in the growth-plane and formation of dipoles along the *c*-axis, respectively.

Fig. 10 shows the polar plots of the interband optical transition rates between the valence and the conduction bands projected on the *x-y* and the *x-z* planes. Noticeable are the suppression in the transition rate and the polarization induced optical anisotropy, which results from the spatial irregularity and the localization of the wavefunctions in the *x-y* and *x-z* planes, respectively (as shown in the insets). Here, the single-particle energies and wave functions are calculated using an empirical nearest-neighbor 20-band $sp^3d^5s^*$ tight-binding model (Sundaresan *et al.* 2014). The energy bandgap of the active disk region, including the effects of quantum size quantization and

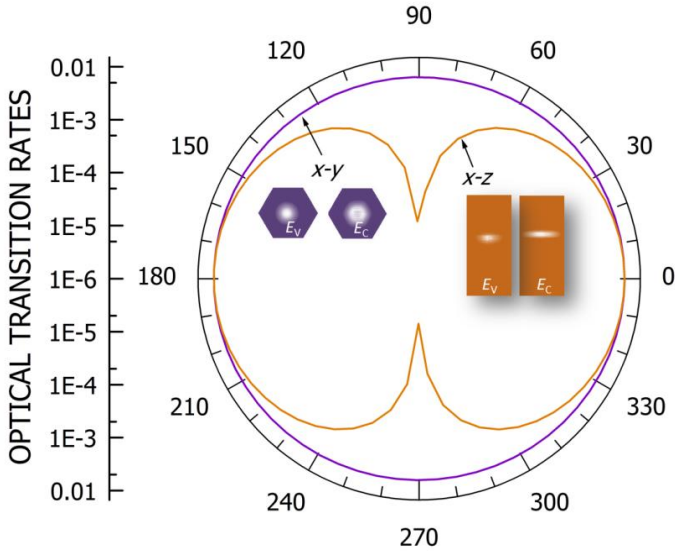

Fig. 10 Interband optical transition rates projected on *x-y* and *x-z* planes

internal fields, is ~4.47 eV and exhibits a blue-shift of ~1.07 eV when compared to the bulk bandgap of GaN (~3.4 eV). The optical anisotropy is quantified via the calculation of polarization ratios ($r = \frac{|I_{\max} - I_{\min}|}{|I_{\max} + I_{\min}|}$), which were found to be 0.0885 and 0.99 in the *x-y* and the *x-z* planes, respectively.

5. Conclusions

Bandstructure of a solid originates from the wave nature of particles (electrons) and depicts the allowed and forbidden energy states of electrons in the material. The knowledge of the bandstructure is the first and essential step towards the understanding of the carrier transport within and reliable design of semiconductor devices. The multimillion-atom *open source* NEMO 3-D software toolkit, currently, lacks a framework for bond passivation for the surface atoms in the calculation of electronic bandstructures of *bare/uncovered* III-V wurtzite nanowires. To address this issue, in this work, we have extended the NEMO 3-D software and employed a systematic approach of constructing the Hamiltonian matrix where the surface dangling bonds are passivated via sp^3 hybridization. It is demonstrated that the surface atoms, if left unpassivated, can lead to the creation of undesirable energy states within the bandgap thus affecting the performance of electronic devices made out of these nanostructures. Note that, the tight-binding model, as implemented in the NEMO 3-D toolkit, generally assumes hard-wall boundary conditions on the interfaces/surfaces. In reality, however, the structure near the surface is altered from the perfect wire structure. The effects of surface reconstruction (with the number of dangling bonds in the surface atoms varying in the quantization direction) on the electronic bandstructure, within a tight-binding formalism, will be the subject of a future work. As for the optical emission characteristics,

it is demonstrated that true atomistic symmetry, and not simply the geometric shape symmetry, coupled with quantum mechanical size quantization in the active disk leads to large reduction of optical transition rates and pronounced anisotropy in the emission characteristics and thus greatly influences the optical performance of the device.

Acknowledgments

This work was supported by the National Science Foundation Grant No. 1102192 and partially by Grant No. 1218839. Computational resources on XSEDE and ORNL Jaguar (through the 2009 ORAU HPC Award) were used for part of this work. The NEMO 3-D package is maintained primarily by Gerhard Klimeck at the Network for Computational Nanotechnology (NCN) at Purdue University West Lafayette. Discussions with Neophytou Neophytos are also acknowledged.

References

Ahmed, S., Islam, S. and Mohammed, S. (2010), "Electronic structure of InN/GaN quantum dots: Multimillion atom tight-binding simulations", *IEEE Tran. Elect. Dev*., **57**(1), 164-173.

Ahmed, S., Yalavarthi, K., Gaddipati, V., Muntahi, A., Sundaresan, S., Mohammed, S., Islam, S., Hindupur, R., John, D. and Ogden, J. (2011), "Quantum atomistic simulations of nanoelectronic devices using QuADS", *Nano-Electronic Devices: Semiclassical and Quantum Transport Modeling*, Springer, Eds. D. Vasileska and S. M. Goodnick, 405-441.

Ahmed, S., Kharche, N., Rahman, R., Usman, M., Lee, S., Ryu, H., Bae, H., Clark, S., Haley, B., Naumov, M., Saied, F., Korkusinski, M., Kennel, R., Mclennan, M., Boykin, T.B. and Klimeck, G. (2009), "Multimillion atom simulations with NEMO 3-D", Meyers, Ed. Robert, *Encyclopedia of Complexity and Systems Science*, **6**, Springer, New York.

Ahmed, S., Usman, M., Heitzinger, C., Rahman, R., Schliwa, A. and Klimeck, G. (2007), "Atomistic simulation of non-degeneracy and optical polarization anisotropy in zincblende quantum dots", *Technical proceedings of the 2nd IEEE International Conference on Nano/Micro Engineered and Molecular Systems*, Bangkok, January.

Bardoux, R., Guillet, T., Gil, B., Lefebvre, P., Bretagnon, T., Taliercio, T., Rousset, S. and Semond, F. (2008), "Polarized emission from GaN/AlN quantum dots: Single-dot spectroscopy and symmetry-based theory", *Phys. Rev. B*, **77**, 235315.

Haley, B.P., Lee, S., Luisier, M., Ryu, H., Saied, F., Clark, S., Bae, H. and Klimeck, G. (2009), "Advancing nanoelectronic device modeling through peta-scale computing and deployment on nanoHUB", *J. Phys. Conf. Ser.*, **180**, 012075.

Hosoya, H., Kido, F. and Tokita, S. (1998), "A new view of hybridized atomic orbitals from *n*-dimensional world", *Croat. Chem. Acta*, **23**(1-2), 169178.

Huang, C.T. , Song, J., Tsai, C.M., Lee, W.F., Lien, D.H., Gao, Z., Hao, Y., Chen, L.J. and Wang, Z.L. (2010), "Single-InN-nanowire nanogenerator with Up to 1 V output voltage", *Adv. Mater.*, **22**, 4008-4013.

Jancu, J.M., Bassani, F., Della Sala, F. and Scholz, R. (2002), "Transferable tight-binding parametrization for the group-III nitrides", *Appl. Phys. Lett*., **81**, 4838.

Klimeck, G., Oyafuso, F., Boykin, T., Bowen, R. and Allmen, P. von. (2002), "Development of a nanoelectronic 3-D (NEMO 3-D) simulator for multimillion atom simulations and its application to alloyed quantum dots", *Comput. Model. Eng. Sci.*, **3**, 601.

Klimeck, G., Ahmed, S., Bae, H., Kharche, N., Rahman, R., Clark, S., Haley, B., Lee, S., Naumov, M., Ryu,

H., Saied, F., Prada, M., Korkusinski, M. and Boykin, T. B. (2007), "Atomistic simulation of realistically-sized nanodevices using NEMO 3-D—Part I: Models and Benchmarks", *IEEE Tran. Elect. Dev*., **54**, 2079-2089.

Klimeck, G., Ahmed, S., Kharche, N., Korkusinski, M., Usman, M., Prada, M. and Boykin, T.B. (2007), "Atomistic simulation of realistically-sized nanodevices using NEMO 3-D-Part II: Applications", *IEEE Tran. Elect. Dev*., **54**, 2090-2099.

Keating, P. (1966), "Effect of invariance requirements on the elastic strain energy of crystals with application to the diamond structure", *Phys. Rev*., **145**.

Li, X., Wang, X., Bondokov, R., Morris, J., An, Y.H. and Sudarshan, T.S. (2005), "Micro/nanoscale mechanical and tribological characterization of SiC for orthopedic applications", *J. Biomed. Mater. Res. Part B: Appl. Biomater.*, **72**(B), 353-361.

Lin, Y.F., Song, J.H., Ding, Y., Liu, S.Y. and Wang, Z.L. (2008), "Piezoelectric nanogenerator using CdS nanowires", *Appl. Phys. Lett*., **92**, 022105.

Lowdin, P.O. (1950), "On the non-orthogonality problem connected with the use of atomic wave functions in the theory of molecules and crystals", *J. Chem. Phys.*, **18**, 365-375.

Lu, M.Y., Song, J.H., Lu, M.P., Lee, C.Y., Chen, L.J. and Wang, Z.L. (2009), "ZnO-ZnS hererojunction and ZnS nanowire arrays for electricity generation", *ACS Nano*., **3**(2), 357-362.

Ma, R.M., Dai, L., Huo, H.B., Xu, W.J. and Qin, G.G. (2007), "High-performance logic circuits constructed on single CdS nanowires", *Nano Lett.*, **7**(11), 3300-3304.

Merrill, K., Yalavarthi K. and Ahmed, S. (2012), "Giant growth-plane optical anisotropy in *c*-plane wurtzite GaN/InN/GaN dot-in-nanowires", *Superlat. Microstr.*, **52**(5), 949-961.

Nakamura, H.S., Senoh, M., Nagahama, S., Iwasa, N., Yamada, T., Matsushita, T., Kiyoku, H., Sugimoto, Y., Kozaki, T., Umemoto, H., Sano, M. and Chocho, K. (1998), "Continuous-wave operation of InGaN/GaN/AlGaN-based laser diodes grown on GaN substrates", *Appl. Phys. Lett.*, **72**.

Neophytou, N. (2008), "Quantum and atomistic effects in nanoelectronic transport devices", Ph.D. Dissertation, Purdue University, Purdue.

Ponce, F. and Bour, D. (1997), "Nitride-based semiconductors for blue and green light-emitting devices", *Nature*, **386**, 351-359.

Prodhomme, P.Y., Beya-Wakata, A. and Bester, G. (2013), "Nonlinear piezoelectricity in wurtzite semiconductors", *Phys. Rev. B*, **88**, 121304(R).

Shur, M.S. and Gaska, R. (2010), "Deep-ultraviolet light-emitting diodes", *IEEE Tran. Elec. Dev.*, **57**(1), 164-173.

Slater, J.C. and Koster, G.F. (1954), "Simplified LCAO method for the periodic potential problem", *Phys. Rev.*, **94**, 1498-1524.

Sundaresan, S., Gaddipati, V. and Ahmed, S. (2014), "Effects of spontaneous and piezoelectric polarization fields on the electronic and optical properties in GaN/AlN quantum dots: Multimillion-atom $sp^3d^5s^*$ tight-binding simulations", *Int. J. Numer. Model.*, Online in Wiley Online Library (wileyonlinelibrary.com). DOI: 10.1002/jnm.2008.

Usman, M., Tan, Y.H.M., Ryu, H., Ahmed, S., Krenner, H.J., Boykin, T.B. and Klimeck, G. (2011) "Quantitative excited state spectroscopy of a single InGaAs quantum dot molecule through multi-million atom electronic structure calculations", *Nanotechnol.*, **22**, 315709.

Yalavarthi, K., Chimalgi, V. and Ahmed, S. (2014), "How important is nonlinear piezoelectricity in wurtzite GaN/InN/GaN disk-in-nanowire LED structures?" *Opt. Quant. Electron.*, **46**, 925-933.

JL